Journal of Cleaner Production 209 (2019) 1016–1024

Contents lists available at ScienceDirect

Journal of Cleaner Production

journal homepage: www.elsevier.com/locate/jclepro

Magnetic valorization of biomass and biochar of a typical plant nuisance for toxic metals contaminated water treatment

Rebone P. Mohubedu, Paul N.E. Diagboya*, Cyprian Y. Abasi, Ezekiel D. Dikio, Fanyana Mtunzi

Applied Chemistry and Nanoscience Laboratory, Department of Chemistry, Vaal University of Technology, Vanderbijlpark, South Africa

ARTICLE INFO

Article history:
Received 9 August 2018
Received in revised form
16 October 2018
Accepted 19 October 2018
Available online 23 October 2018

Keywords:
Acorn (*Quercus robur*) fruit biomass
Biochar
Magnetic biomass
Magnetic biochar
Adsorption
Pb(II) and Cd(II)

ABSTRACT

Low-cost materials are promising aqueous pollutant adsorbents but when batch adsorption method is employed, separation of pollutant-loaded-adsorbents from water is a major challenge especially when dealing with a large volume of wastewater. Thus, biomass and biochar from *Quercus robur* fruits were valorized via magnetization (for easy post-adsorption separation) to prepare optimized biomass-magnetic hybrid (BMM 0.5:1) and biochar-magnetic hybrid (BCM 1:1). The BMM 0.5:1 and BCM 1:1 were employed for Pb(II) and Cd(II) removal from simulated contaminated water. The hybrids exhibited higher values of cation exchange capacity (CEC), BET surface area and pore sizes, as well as better thermal stability and the presence of pure spinal structures of Fe_3O_4, along with the characteristic functional groups of biomaterials (such as the hydroxyls, amides and carboxyls). The adsorption equilibria for both cations were attained within 180 min. Adsorption mechanism involved electrostatic interactions on both external and pore surfaces, with Pb(II) data fitting the Langmuir adsorption isotherm model while Cd(II) data fitted the Freundlich. The adsorption process was spontaneous and exothermic as solution temperature was increased from 292 to 310 and 328 K. The adsorption of Cd(II) initially increased with temperature but decreased on further temperature rise by similar percentages for both adsorbents. In contrast, adsorption of Pb(II) decreased continuously but the decrease was higher for BMM 0.5:1 than BCM 1:1 implying BCM is a more promising adsorbent. Adsorption capacities for BMM 0.5:1 are 63.6 and 21.0 mg/g, while BCM 1:1 has 58.2 mg/g and 21.3 mg/g for Pb(II) and Cd(II), respectively. These adsorption capacities were better than many low-cost adsorbents in literature. Thus magnetic valorization, apart from easing separation, enhances the adsorption capacity of low-cost adsorbents.

1. Introduction

The volume of wastewater currently generated and dispersed within receiving water bodies is unprecedented; in fact, an estimated 42% of the world's population lack proper sanitation facilities, while another 18% do not have access to any type of improved drinking water facility – more than one out of six persons lack access to safe drinking water (Olu-Owolabi et al., 2017). Hence, the need for wastewater treatment cannot be overestimated especially in urban centers.

Wastewater contains numerous toxic chemical pollutants. The array is limitless and includes plastics and soluble chemical substances like persistent organic pollutants and toxic metals (Diagboya and Dikio, 2018a). For the sake of this study, we focused on two model pollutants, Pb(II) and Cd(II), which are two of the most commonly found toxic metals in water. Pb(II) is linked to disorders such as nervous breakdown while Cd(II) has been linked to bone demineralization (Wang et al., 2015).

Several adsorption-based wastewater treatment techniques have been employed because of their techno-economic and environmental advantages over other techniques like precipitation, ion exchange, electrochemical treatment and membrane technology. Such advantages include: low-cost and availability of adsorbent as waste or nuisance, ease of technique application, ease of tuning surface functional groups of the adsorbents, regeneration of used adsorbents, tunable adsorption efficiency and environmental friendliness (Diagboya and Dikio, 2018b). Using low-cost

* Corresponding author.
E-mail address: pauldn2@yahoo.com (P.N.E. Diagboya).

https://doi.org/10.1016/j.jclepro.2018.10.215

adsorbents which are available as wastes or nuisance is of particular environmental importance because it reduces their undesirable effects in the environment. For instance, acorn (*Quercus robur*) tree is usually used as an ornamental plant in gardens around the world and it is especially common in Vanderbiljpark, South Africa. Nevertheless, the mature acorn tree produces several tonnes of its fruit annually which constitute nuisance in the environment. Utilizing this large amount of acorn fruits as adsorbent would be an important way of remedying the environmental issue as well as treating wastewater.

Several studies, including those of Anandkumar and Mandal (2011), Okoli et al. (2017) and Russo et al. (2010), on adsorption-based techniques employ low-cost and waste-type adsorbents for aqueous pollutant removal via the batch adsorption method. Though they have shown promising results, a major challenge is the separation of pollutant-loaded-adsorbent from the aqueous solution after the adsorption process. The conventional filtration and centrifugation-based techniques are cumbersome, not cost-effective and sometimes difficult to handle, and these challenges are considerable when dealing with a large volume of waste. Thus, there is need to design more effective batch process by eliminating these challenges.

Low-cost adsorbent magnetization represents a potential effective method of separating used adsorbents from treated water. The process involves magnetizing the adsorbent which is then used for the batch adsorption. The magnetized adsorbent is then removed from solution after the adsorption process by using a magnetic field to separate the used magnetized adsorbents from solution. Similar magnetic procedure has been reported for separating adsorbent materials from solution (Hao et al., 2010; Kang et al., 2011; Nassar, 2010; Tian et al., 2009); however, most preparation methods are not cost-effective, use very high temperatures and not simple. Hence, the aim of this study was the preparation of cost-effective, benign and simple magnetic valorization of raw biomass and biochar adsorbents, sourced from waste acorn fruit biomass, for removal of Pb(II) and Cd(II) in simulated aqueous solutions. Data generated from this study have been analyzed to determine the adsorbents adsorption capacities as well as the adsorption mechanisms involved.

2. Materials and methods

2.1. Materials, biomass sampling and pretreatment

Analytical grade reagents (lead chloride, cadmium chloride, ferric and ferrous chloride salts (Aldrich)) were used throughout this study. *Quercus robur (*acorn) fruits (Fig. 1 insert) were obtained from ornamental gardens around Vaal University of Technology South Africa and pretreated by separating the pericarp from the cotyledon. Both parts were then washed with tap water, dried at 105 °C to constant weight and pulverized to fineness using a steel blender, followed by sieving through a 230 μm mesh size sieve. The pulverized pericarp and cotyledon were stored separately in air-tight containers prior to the study.

2.2. Sorbents preparation

Specific masses of the pulverized pericarp and cotyledon were charred separately for 4 h in a furnace at 250 °C to obtain their biochar. The biomasses were initially dried at 110 °C for 1 h, temperature was then ramped at a rate of 5 °C/min until 250 °C which was maintained for 4 h. The biochar obtained from the cotyledon was insignificant (≈6%) in mass (mostly ash) compared with the pericarp; thus we did not continue the experiment with cotyledon biochar but used the un-charred (raw) cotyledon. The pericarp biochar (≥33%) was cooled, ground, sieved with a 230 μm mesh, followed by washing until the filtrate was colourless indicating no leaching of residual carbon, dried at 105 °C, cooled, weighed, and biochar stored. Due to durability and better performance the biochar of the biomasses were used whenever possible.

The magnetite–biomass/biochar hybrids were prepared (Fig. 1) from a suspension of the biomass in 400 mL solution of $FeCl_3$ and $FeCl_2$ (molar ratio 2:1) (Diagboya and Dikio, 2018c). This was initially stirred to allow for wetness of the biomass before a 1.0 M NaOH solution was added drop-wise while stirring to raise suspension pH above 9 and co-precipitate the magnetic nanoparticles (MNP) on the biomass. Earlier, the weight of the biomass was adjusted to obtain final biomass or biochar to MNP weight ratios of either 0.5:1, 1:1 or 2:1. The charring experiment above gave details

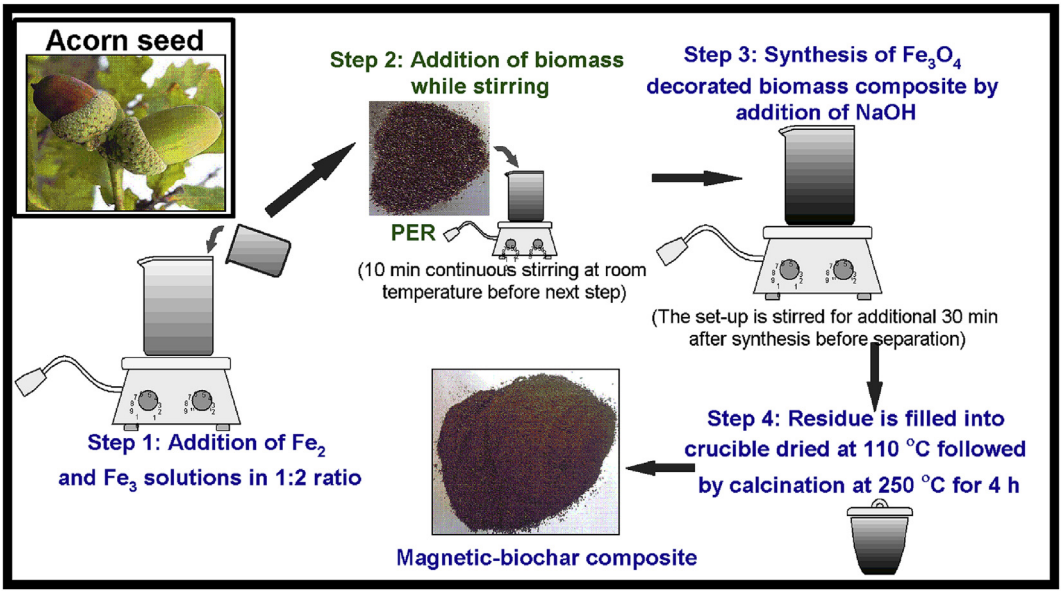

Fig. 1. Magnetic-biomaterials preparation schematics (Insert picture: Acorn seed).

of the required mass to obtain this ratio for the biochar–MNP hybrid. Once the suspension became dark upon NaOH addition, the biomass–MNP solution was further stirred for 1 h before separation from solution and filling of the residue into a crucible for the pyrolysis process using the temperature regime described above. After this, the residues were washed continuously until no Fe and organic residues were leached from the hybrid upon washing. The hybrids were dried and stored, and the magnetic–pericarp biochar was denoted as BCM, while the magnetic–cotyledon biomass was BMM. For this study, the hybrids containing the highest amounts of biomass or biochar while still exhibiting sufficient magnetic properties were chosen; thus the final adsorbents were BCM 1:1 and BMM 0.5:1. These choices were to allow for the maximum and minimum biomaterials and MNP usage, respectively.

The MNP, pericarp and cotyledon biomasses, pericarp biochar, and all ratios of BCM and BMM samples were characterized by determining their pHH_2O, point of zero charge (pHPZC) via the solid addition method and Cation Exchange Capacity (CEC) via the sodium saturation method (Olu-Owolabi et al., 2016a). The infrared spectra (Fourier transform infrared (FTIR) spectrometer– Perkin Elmer Instruments, USA), specific surface area and porosity using the Micromeritics TRISTAR II 3020 analyser (Micromeritics Instrument Corporation, USA), Thermo-gravimetric analysis (TGA; Perkin- Elmer TGA 4000, Perkin Elmer Instruments, USA), *X*-ray diffractograms (*X*-ray diffractometer (XRD)–7000, Shimadzu, Japan) and scanning electron micrographs (SEM; Zeiss Auriga Field Emission Scanning Electron Microscope with Oxford X-max EDX detector) of selected adsorbents were obtained (Igberase et al., 2014).

2.3. Adsorption experimental studies

All adsorption experiments were carried out in replicates by adding 20 mL solution of specified concentration of the pollutant (Pb(II) or Cd(II)) into 50 mL plastic centrifuge tubes containing 20 mg of the adsorbent (Olu-Owolabi et al., 2018). The pollutant/adsorbent mixtures were then equilibrated at 200 rpm on a shaker at 18 ± 1 °C and pH 6.8 ± 0.5 (except where otherwise stated). The working solutions' pH were adjusted when required by adding drops of either 0.1 M HCl or NaOH. At stipulated times or equilibrium, desired tubes were withdrawn, centrifuged at 4000 rpm for 10 min and the concentrations of pollutants left in the supernatants were determined using flame atomic absorption spectrophotometer (F–AAS (AA–7000) Shimadzu, Japan). The effects of the following experimental parameters were studied: time (1–240 min using 100 mg/L of pollutant), pH (3–11; 100 mg/L of pollutant; and 180 min equilibration time), concentration (25–150 mg/L and 180 min), and temperature (19, 37, and 55 °C using similar conditions in effect of concentration).

2.4. Data treatment

The quantity of any pollutant adsorbed at any particle point was determined using $q_e = (C_o - C_e)v/m$, where q_e (mg/g) is the quantity of pollutant adsorbed, C_o and C_e are initial and final pollutants concentrations in solutions, while v (mL) and m (g) are the volume of pollutant solution used and adsorbent mass, respectively.

The nonlinear forms of the pseudo-first order (PFO) (Eq. (1)) and pseudo-second order (PSO) (Eq. (2)) (Lagergren, 1898), and the intra-particle diffusion (IPD) (Eq. (3)) (Weber and Morris, 1963) kinetic models were employed in modeling the data.

$$q_e = q_t(1 - e^{-k_1 t}) \quad (1)$$

$$q_e = \frac{1 + k_2 q_e t}{k_2 q_e^2 t} \quad (2)$$

$$q_t = k_i(t^{1/2}) + C \quad (3)$$

The model parameters were obtained using KyPlot software where q_e (mg/g) and q_t (mg/g) denote quantities of pollutants adsorbed at equilibrium and time t; and k_1 (min^{-1}) and k_2 (g $mg^{-1}min^{-1}$) are the PFO and PSO rate constants, respectively. The rate parameter of the IPD is k_{IPD} (g/g $min^{1/2}$) while C is the pollutants' surface concentration on the adsorbent.

Equilibrium data were fitted to the Langmuir (1916) (Eq. (4)) and Freundlich (1906) (Eq. (5)) adsorption isotherm models.

$$q_e = \frac{Q_o b C_e}{1 + bC_e} \quad (4)$$

$$q_e = k_f C_e^{1/n} \quad (5)$$

The variables Q_o is the maximum adsorption capacity per unit weight of adsorbent (mg/g), b is energy-related to solute–surface interaction, k_f is Freundlich model capacity factor, $1/n$ the isotherm linearity parameter, while other parameters are same as above.

Thermodynamic parameters of enthalpy (ΔH°), entropy (ΔS°), and Gibbs free energy (ΔG°) were determined from data at 292, 310, and 328 K as described in an earlier article (Diagboya and Dikio, 2018c) and R, the ideal gas constant, was taken as 8.314 J/mol K.

3. Results and discussion

3.1. Adsorbent physicochemical characterizations

The magnetic valorization of biosorbents sourced from a typical ornamental seed waste or nuisance have been carried out in this study. The inner fruity cotyledon (raw biomass) and the cellulosic pericarp (processed into biochar) have been magnetized using magnetic nanoparticles (MNP) at varying weight ratios to the biomaterials in order to fabricate the magnetic biosorbents. The various weight ratios used for both the raw and biochar adsorbents are 0.5:1, 1:1 and 2:1. In this study, we regard a magnetic adsorbent as useful if it has the highest amount of biomass or biochar while still exhibiting good magnetic properties. Thus, the final two adsorbents chosen from both categories were BCM 1:1 and BMM 0.5:1. The aim of the magnetization was to enhance adsorption properties and ease adsorbents removal after the adsorption.

In order to appropriately describe the chemical, physical and adsorption properties of the adsorbents, they have been characterized using established methods as stated above and the results are shown in Table 1, Fig. 2 and SM Figs. 1–4. The results indicated enhanced cation exchange capacity (CEC), BET surface area and pore size values for both BCM 1:1 and BMM 0.5:1 when compared with the starting low-cost biomaterials (Table 1), though lower than the pure MNP. These enhanced values were suggestive of better adsorption properties with higher cation exchange both on the external and internal surfaces/pores (Diagboya and Dikio, 2018c). The BCM 1:1 and BMM 0.5:1 adsorbents have both pH_{H2O} and pH_{PZC} values which are close to each other but were slightly alkaline (≈8.8) and acidic (≈4.3), respectively. Both parameters affect cations adsorption in solution because they determine the

Table 1
Physicochemical characteristics of pre- and post-fabricated adsorbents.

Adsorbent	pH_{H2O}	pHpzc	CEC (cmol/kg)	BET Surface area (m^2/g)	Pore size (cm^2/g)	Comment
MNP	10.34	9.81	9.16	72.90	0.17	Strong *M
Pericarp	6.66	6.57	5.56	0.014	–	No M
Pericarp Biochar	7.16	7.08	7.48	0.63	–	No M
Cotyledon Biomass	5.73	5.49	10.23	0.01	–	No M
BMM 0.5:1	4.56	3.99	10.23	37.60	0.11	Good M and *B
BMM 1:1	8.48	7.89	6.53	37.79	0.07	Poor M
BCM 0.5:1	9.54	9.32	5.59	50.27	0.16	Good M; Low B
BCM 1:1	8.90	8.66	9.34	42.24	0.15	Good M and B
BCM 2:1	8.63	8.53	8.55	32.97	0.11	Poor M

* CEC– cation exchange capacity; *M– Magnetism; *B– Biomaterial.

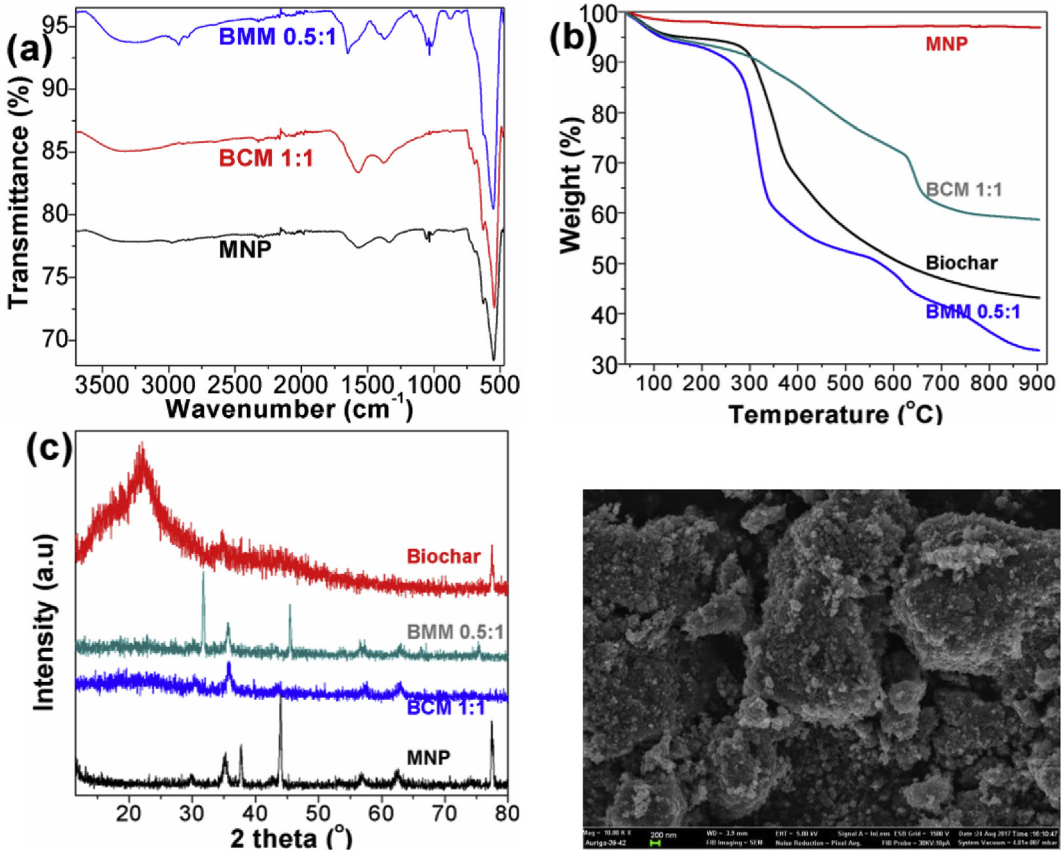

Fig. 2. Spectra from (a) FTIR, (b) TGA, and (c) XRD analysis, (d) SEM of BMM 0.1:1.

charge state of the adsorbent.

The infra-red spectra peaks were scanned between 4000 and 450 cm^{-1} for all biosorbents (Fig. 2a, SM Figs. 1–3). The characteristics peaks associated with biomass-sourced adsorbents were observed (SM Fig. 1) for hydroxyl (≈3400 cm^{-1}), amides (≈1640 cm^{-1}), carboxyl, carbonyl, methyl ketone, aromatic methyl groups, and possibly C–H deformations of alkane (≈1400 to 1000 cm^{-1}) and, major plane group deformations and thioesters groups (<1000 cm^{-1}) (Asuquo and Martin, 2016; Okoli et al., 2017). Notably, the characteristic intense peak of Fe–O bond from the iron oxide in MNP was expressed in Fig. 2a (SM Fig. 1– *MNP*) spectra at 547 cm^{-1} (Chen et al., 2011; Diagboya et al., 2015a). This peak became expressed in all magnetic adsorbents as shown in Fig. 2a (SM Figs. 2 and 3); this is an indication of the presence of Fe–O bond within the hybrid adsorbents which impacted magnetic properties on them.

The thermogravimetric analysis (TGA) spectra of the MNP, biochar and BCM 1:1 and BMM 0.5:1 are shown in Fig. 2b. The TGA was carried out in the temperature range of ≈40 to 900 °C. The spectra showed that the MNP was very stable losing only <5% mass at 900 °C, while the biochar was not as stable losing ≈58% of its mass at the same temperature. Loss of trapped or embedded water molecules in the MNP, biochar and adsorbents were observed at ≤120 °C. This was followed by significant volatilization of part of the labile oxygen-containing groups and stable backbone structures of the biomass and biochar starting around 180 °C for BMM and increasing drastically from 250 °C for both BMM and BCM. A total weight loss of approximately 40 and 68% were observed for both adsorbents, respectively. The TGA showed that stability of the BCM was greater than that of the BMM by ≈ 30% mass.

Powder *XRD* of the biochar and hybrids adsorbents are shown in Fig. 2c (SM Fig. 4). The biochar exhibited typical amorphous powder

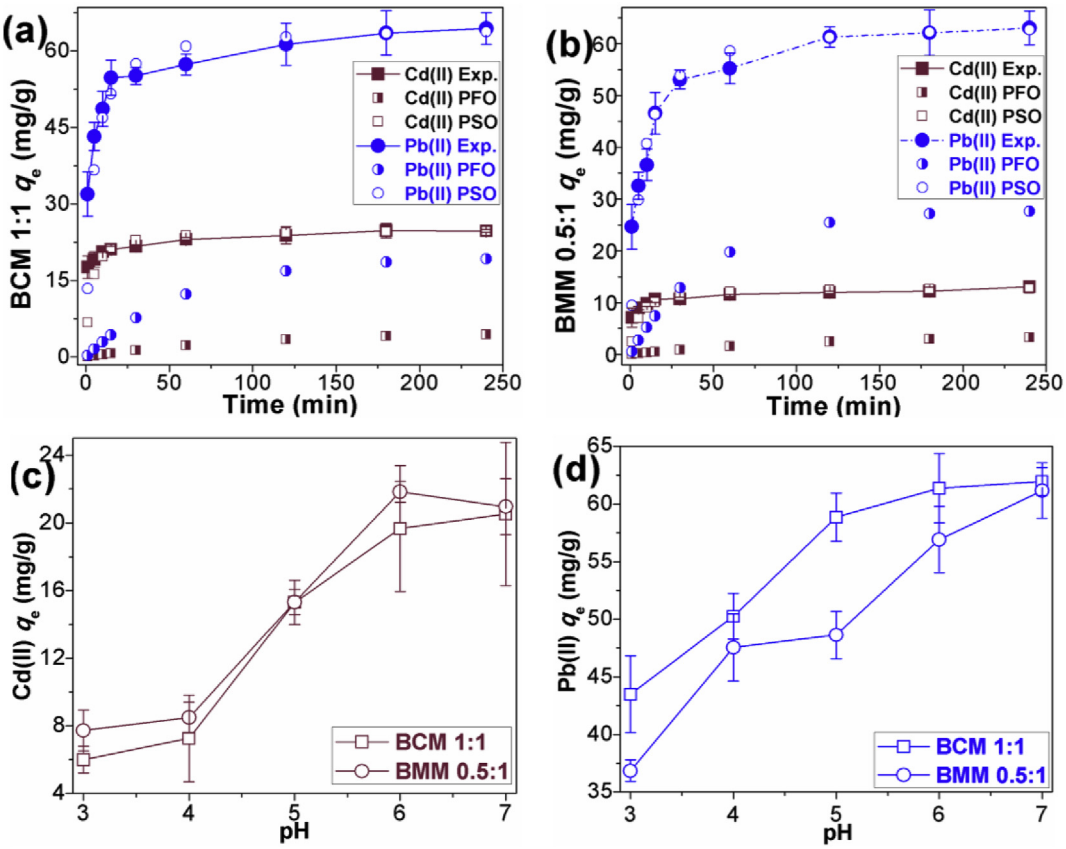

Fig. 3. Adsorption trends as time varied for Pb(II) and Cd(II), and pseudo-first order (PFO) and pseudo-second order (PSO) kinetic fittings for (a) BCM 1:1 and (b) BMM 0.5:1 adsorbents; adsorption trends for (c) Cd(II) and (d) Pb(II) as pH varied.

spectra (Castro et al., 2009). In the MNP diffractogram, the presence of pure spinal structures of Fe_3O_4 at 2-theta values of 29.8, 35.2, 43.1, 56.8, 62.6, and 77.4° are indicative of characteristic peaks of MNP (Castro et al., 2009; Diagboya and Dikio, 2018c; Zhang et al., 2013). The spectra patterns of the all magnetic adsorbents exhibited these characteristic MNP peaks albeit with slight shifts in instances (Fig. 2c; SM Fig. 4). The SEM images (Fig. 2*d*; SM Fig. 5) of both hybrids showed MNP distributed on the surfaces of both the raw and charred biomass (Castro et al., 2009).

3.2. Adsorbent kinetic

The trends for the adsorption rates of Pb(II) and Cd(II) ions by both BCM 1:1 and BMM 0.5:1 hybrid adsorbents are shown in Fig. 3*a*–*b* (trend lines with filled marks). The trends showed fast removal rates for both cations within 30 min of initiating the adsorption process, while a stable equilibrium was attained for both adsorbents within 180 min. The fast rates associated with the initial 30 min of the adsorption process were ascribed to adsorption on easily accessible functional groups on the empty surface adsorption sites on these adsorbents (Bulgariu and Bulgariu, 2016). Once the empty surface adsorption sites are filled, pore surfaces adsorption and entrapment within the interstitial spaces begin but at slower rates due to difficulty of the cations permeating these spaces; thus the nature of the curves between 30 and 120 min. At equilibrium, the adsorption was stable within the range of the standard deviations (plateau of the curve).

The rates data for Pb(II) and Cd(II) ions adsorption on the hybrid magnetic adsorbents were evaluated by the pseudo–first order (PFO), pseudo–second order (PSO), and the intra-particle diffusion (IPD) kinetic models. This was in order to predict the possible adsorption mechanism(s) for both cations on these hybrids. The model fittings and calculated parameters are shown in Fig. 3*a*–*b* and Table 2, respectively. The nonlinear fittings (Fig. 3*a*–*b*) of the Pb(II) and Cd(II) cations adsorption data obtained using the *KyPlot* software shows that the PSO model (half filled markers without trend lines) described the data better than the PFO model for both cations and hybrids. The PFO model exhibited under-estimations of both cations adsorption data. The detailed kinetic parameters of both models shown in Table 2 give meaningful explanations for these fittings. In agreement with the *KyPlot* fittings, the PSO correlation coefficients (r^2) were very close to unity (0.997–0.999) while the calculated model q_e values were similar to the experimentally obtained values. On the other hand, the PFO model showed lower r^2 values (0.821–0.955) with very low underestimated q_e values. The better fit of the PSO (higher r^2 and q_e values close to experimental) is suggestive of a mechanism that involves electrostatic interactions between the cations from solution and the negatively charged functional groups on the empty adsorption surfaces (Olu-Owolabi et al., 2016b).

Table 2 also shows parameters for the IPD kinetic model. The model also gives details of the nature of the removal processes. For instance, the C (mg/g) value suggests where the adsorption occurred on the adsorbent – surface or within pores or partitions. This value indicates the surface thickness of the adsorbed species; when equal to the experimental q_e value, it implies the adsorption process occurred majorly on the adsorbent surface. The C (mg/g) values from this study showed that both surface and pore adsorption played vital roles in both cations removal processes with surface adsorption being more prominent for Cd(II) (ESA

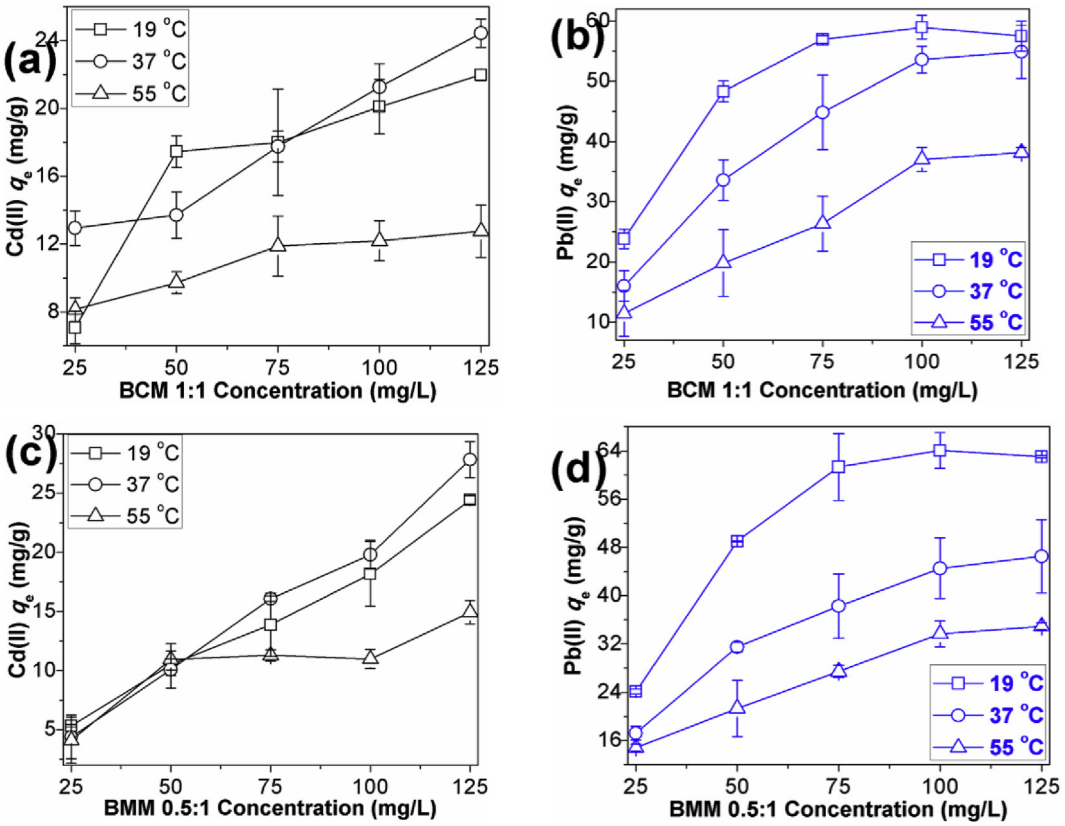

Fig. 4. (a) Cd(II) and (b) Pb(II) adsorption trends on BCM 1:1; (c) Cd(II) and (d) Pb(II) adsorption trends on BMM 0.5:1 at 19, 37, and 55 °C.

Table 2
BCM 1:1 and BMM 0.5:1 kinetic model parameters for Pb(II) and Cd(II) adsorption.

Kinetic model	Parameter	Cd(II) on BCM 1:1	Cd(II) on BMM 0.5:1	Pb(II) on BCM 1:1	Pb(II) on BMM 0.5:1
*PFO	q_e (mg g^{-1})	4.73	3.66	19.61	27.84
	k_1 (min^{-1})	−0.011	−0.010	−0.017	−0.021
	r^2	0.829	0.821	0.930	0.955
*PSO	q_e (mg g^{-1})	24.92	12.89	64.78	64.21
	k_2 (g mg^{-1}min^{-1})	0.015	0.018	0.004	0.003
	r^2	0.999	0.997	0.999	0.999
*IPD	C (mg g^{-1})	18.64	8.401	40.89	31.00
	k_i (g g^{-1} min$^{1/2}$)	0.453	0.321	1.771	2.465
	r^2	0.890	0.818	0.756	0.819
*EPA	%	23.6	32.3	35.2	50.2
*ESA	%	76.4	67.8	64.8	49.8
Experimental	mg/g	24.4	12.4	63.1	62.2

*Pseudo-first order (PFO) kinetic model; *Pseudo-second order (PSO) kinetic model; *Intra-particle diffusion (IPD) kinetic model; *EPA = Estimated pore adsorption of IPD; ESA = Estimated surface adsorption of IPD.

≥67%) than Pb(II) (ESA ≥49%).

3.3. Effect of pH on Pb(II) and Cd(II) ions adsorption

The cation solution pH is one major variable that affects the adsorption process. The cation solution pH affects the charge density on the adsorbent's adsorption sites which influences the extent of adsorption, as well as ionization state of the pollutant (Asuquo and Martin, 2016). In order to ascertain the effect of pH on these hybrids adsorption of both cations, the effect of pH was probed as described above and the results are depicted in Fig. 2 *c–d*. The results showed that the adsorption process for both cations were pH dependent and increased with pH until optimum adsorption was attained between pH 6 and 7 for Pb(II) and Cd(II); thus, both cations had similar trend. This adsorption trend could be explained in terms of the influence of pH on the charge density on the hybrids' adsorption sites. At the lowest solution pH value used for the experiments (pH 3), the degree of ionization of surface functional groups on adsorption sites are very low. The high concentration of protons (H^+) in solution at this pH also enhances this low ionization state, as well as behaves as competing group for the negatively charged site (Okoli et al., 2017). Thus, in the absence or low amounts of negatively charged functional groups and high amount of H^+, electrostatic interaction (predicted to be the major mechanism of cation adsorption) is low, resulting in low adsorption. However, as pH increases, ionization of the negatively charged sites/groups increases and the competition from H^+ for such groups becomes less potent, resulting in increased electrostatic attraction

and adsorption increases consequently.

3.4. Equilibrium, temperature studies and adsorption isotherm modeling

Equilibrium studies on both adsorbents using varying concentrations of Pb(II) and Cd(II) were carried out and adsorption trends are shown in Fig. 4 *a–d*. The trends expressed increased adsorption as concentrations were increased for both cations. The observed trend was attributed to the enhanced adsorption which occurs when adsorbate concentration is increased at the point of equal movement of cations between the external surface film and internal pores (Diagboya and Dikio, 2018c), and possibly due to multilayer adsorption.

The cations adsorption exhibited different trends for Pb(II) and Cd(II) as the temperature was varied (Fig. 4 *a–d*). As temperature increased from 292 to 310 K, Cd(II) adsorption trend increased by approximately 10% for both adsorbents, but further temperature increase to 328 K resulted in approximately 40% decrease in adsorption. However, Pb(II) adsorption decreased continuously with increased temperature from 292 to 310 and 328 K by approximately 7 and 35% for BCM 1:1, and 28 and 46% for BMM 0.5:1, respectively. Thus, while Cd(II) adsorption initially increased with temperature and then later decreased for both adsorbents, the Pb(II) adsorption decreased continuously, but the decrease was higher in BMM 0:1 than for BCM 1:1 implying BCM is a more promising adsorbent. These trends were irrespective of the biomass nature, that is, whether raw biomass or the biochar. The trend for Cd(II) was attributed to the fact that it is retained by exchange reactions which were enhanced (reduced activation energy) by initial temperature rise, but further rise resulted in higher adsorbate entropy and reduced adsorption. However, Pb(II) removal is basically via inner sphere complexation with organic matter but the increased entropy associated higher temperature meant that fewer of these weak complexes were formed and hence the lower removal quantities (Diagboya et al., 2015b; Lu and Xu, 2008).

The Pb(II) and Cd(II) equilibrium data at the various temperatures were evaluated for the thermodynamic parameters as shown in Table 3 in order to predict the nature of the adsorption process. The calculated negative ΔH° values indicated exothermic processes and supported the reduced cations adsorption observed with increased input of external energy, while the mostly positive ΔS° values suggested increased randomness for cations in solution as the adsorption moved towards equilibrium. The negative ΔG° values were indicative of spontaneous adsorption processes for both cations. The small positive ΔG° values observed in a few cases may be attributed to inherent errors in the linear model thermodynamic parameters calculation which become significant for low energy surfaces (Diagboya et al., 2018).

The equilibrium data at 292 K were evaluated using the Langmuir and Freundlich adsorption isotherm models and the isotherm parameters are shown in Table 4. It was observed that the Pb(II) adsorption on both hybrids were better described by the Langmuir adsorption isotherm model with r^2 values of 0.999 and Q_o values that were equal to the experimentally obtained values. This good fit was suggestive of monolayer Pb(II) adsorption on adsorption sites with almost equal affinity for Pb(II) cation (Asuquo and Martin, 2016). The adsorption of Cd(II) on the other hand fit better to the Freundlich adsorption isotherm model with r^2 values ≥ 0.894. This model proposes that Cd(II) adsorption on these hybrids occurred on heterogeneous surfaces of unequal energy and that multilayer adsorption might have occurred on the initial surface adsorbates at equilibrium (Asuquo and Martin, 2016).

In corroboration of our earlier report (Diagboya and Dikio, 2018c), the magnetic valorization, apart from easing the removal of spent adsorbents from treated water, enhanced the adsorption capacity of the hybrid adsorbents. In general, faster adsorption rates were observed for Pb(II) compared to the Cd(II) on both adsorbents. Also, comparing adsorption on both adsorbents showed better adsorption on the biochar hybrid (BCM 1:1) than the raw biomass hybrid (BMM 0.5:1), with higher adsorption for Pb(II) than Cd(II). The hybrids adsorption capacities for Pb(II) and Cd(II) were compared with some other low-cost adsorbents in literature in order to evaluate their effectiveness (Table 5). Table 5 showed that these hybrid adsorbents were better than several low-cost adsorbents reported in literature.

4. Conclusion

Biomass and biochar were valorized by magnetization via a facile and benign process to prepare BMM 0.5:1 and BCM 1:1, respectively. Both hybrids exhibited higher cation exchange capacity, BET surface area and pore sizes than the starting low-cost biomaterials. The adsorption of Pb(II) and Cd(II) ions by the hybrids involved electrostatic interactions between the cations and the negatively charged functional groups on the empty adsorption

Table 3
Thermodynamic parameters for Pb(II) and Cd(II) adsorption.

Thermodynamic Parameter		Cd(II) BCM 1:1	Cd(II) BMM 0.5:1	Pb(II) BCM 1:1	Pb(II) BMM 0.5:1
ΔH°	kJ mol^{-1}	15.37	−3.79	−98.28	−86.11
ΔS°	J mol^{-1} K^{-1}	−48.75	24.10	303.40	260.58
ΔG° (kJ mol^{-1})	292 K	1.58	3.13	−10.51	−10.99
	310 K	−0.76	3.96	−2.36	−3.17
	328 K	−0.06	3.96	0.20	−1.86

Table 4
Langmuir and Freundlich adsorption isotherm models parameters.

Adsorption isotherm model	Parameter	Cd(II) BCM 1:1	Cd(II) BMM 0.5:1	Pb(II) BCM 1:1	Pb(II) BMM 0.5:1
Langmuir	Q_o (mg g^{-1})	33.33	125.00	58.82	66.67
	β	0.02	0.002	2.83	2.50
	r^2	0.875	0.512	0.999	0.999
Freundlich	*1/n*	0.441	0.890	0.118	0.151
	k_f	1.69	0.38	33.07	37.33
	r^2	0.894	0.991	0.498	0.653
Experimental Q_o	mg/g	21.04	21.30	58.22	63.56

Table 5
Comparison of adsorption capacities of the BMF composites with those of similar composites and some low-cost adsorbents.

Adsorbent	Pollutant	q_e (mg/g)	Reference
Bentonite-*Carica papaya* composite	Cd(II)	10.9	(Olu-Owolabi et al., 2016a)
Feldspar-Pine cone composite	Cd(II)	11.5	(Olu-Owolabi et al., 2018)
Feldspar-*Carica papaya* composite	Cd(II)	12.6	(Olu-Owolabi et al., 2018)
Bentonite-Pine cone composite	Cd(II)	12.6	(Olu-Owolabi et al., 2016a)
BMF-0.5	Cd(II)	15.8	(Diagboya and Dikio, 2018c)
BMF-1	Cd(II)	17.8	(Diagboya and Dikio, 2018c)
Sweet potato peels	Cd(II)	18.9	(Asuquo and Martin, 2016)
BMM 0.5:1	Cd(II)	21.0	This study
BCM 1:1	Cd(II)	21.3	This study
Algae Waste Biomass (AWB)	Cd(II)	33.7	(Bulgariu and Bulgariu, 2016)
Alkaline treated−AWB	Cd(II)	41.9	(Bulgariu and Bulgariu, 2016)
Feldspar-*Carica papaya* composite	Pb(II)	26.0	(Olu-Owolabi et al., 2018)
Magnetic chitosan microparticles	Pb(II)	121.3	(Li et al., 2013)
Magnetic xanthate-chitosan	Pb(II)	76.9	(Zhu et al., 2012)
Valonia tannin resin	Pb(II)	52.4	(Şengil and Özacar, 2009)
BMM 0.5:1	Pb(II)	63.6	This study
BCM 1:1	Pb(II)	58.2	This study

surfaces on both the external surfaces and within pores. Adsorption equilibrium was within 180 min while optimum adsorption was attained between pH values of 6 and 7. The Cd(II) adsorption initially increased up to 310 K and then decreased for both adsorbents. However, Pb(II) adsorption decreased continuously but the decrease was higher for BMM 0:1 than BCM 1:1 implying BCM is a more promising adsorbent. Thermodynamic parameters calculations predicted spontaneous and exothermic processes for the cations. The Pb(II) adsorption data for both hybrids suggested monolayer adsorption on almost equal adsorption sites, while Cd(II) adsorption data indicated adsorption on heterogeneous surface sites of unequal energy and possibly multilayer adsorption. In general, faster and higher adsorption rates were observed for Pb(II) compared to the Cd(II) on both adsorbents, while significantly higher adsorption was exhibited by the biochar hybrid (BCM 1:1) more than the raw biomass hybrid (BMM 0.5:1). The hybrids adsorption capacities for Pb(II) and Cd(II) were better than many low-cost adsorbents in literature. The magnetic valorization, apart from easing the removal of spent adsorbents from treated water, enhanced the adsorption capacity of the hybrid adsorbents.

Acknowledgment

We acknowledge the supports of the Department of Chemistry and Research Directorate, Vaal University of Technology, Vanderbiljpark, South Africa.

Appendix A. Supplementary data

Supplementary data to this article can be found online at https://doi.org/10.1016/j.jclepro.2018.10.215.

References

Anandkumar, J., Mandal, B., 2011. Adsorption of chromium(VI) and Rhodamine B by surface modified tannery waste: kinetic, mechanistic and thermodynamic studies. J. Hazard Mater. 186 (2–3), 1088–1096.
Asuquo, E.D., Martin, A.D., 2016. Sorption of cadmium (II) ion from aqueous solution onto sweet potato (Ipomoea batatas L.) peel adsorbent: characterisation, kinetic and isotherm studies. J. Environ. Chem. Eng. 4 (4), 4207–4228.
Bulgariu, D., Bulgariu, L., 2016. Potential use of alkaline treated algae waste biomass as sustainable biosorbent for clean recovery of cadmium(II) from aqueous media: batch and column studies. J. Clean. Prod. 112, 4525–4533.
Castro, C.S., Guerreiro, M.C., Gonçalves, M., Oliveira, L.C.A., Anastácio, A.S., 2009. Activated carbon/iron oxide composites for the removal of atrazine from aqueous medium. J. Hazard Mater. 164 (2–3), 609–614.
Chen, B., Chen, Z., Lv, S., 2011. A novel magnetic biochar efficiently sorbs organic pollutants and phosphate. Bioresour. Technol. 102 (2), 716–723.
Diagboya, P.N., Dikio, E.D., 2018a. Silica-based mesoporous materials; emerging designer adsorbents for aqueous pollutants removal and water treatment. Microporous Mesoporous Mater. 266C, 252–267.
Diagboya, P.N., Dikio, E.D., 2018b. Dynamics of Mercury solid phase extraction using Barbula lambarenensis. Environ. Technol. Innov. 9, 275–284.
Diagboya, P.N., Dikio, E.D., 2018c. Scavenging of aqueous toxic organic and inorganic cations using novel facile magneto-carbon black-clay composite adsorbent. J. Clean. Prod. 180, 71–80.
Diagboya, P.N., Olu-Owolabi, B.I., Adebowale, K.O., 2015a. Synthesis of covalently bonded graphene oxide–iron magnetic nanoparticles and its kinetics of mercury removal. RSC Adv. 5, 2536–2542.
Diagboya, P.N., Olu-Owolabi, B.I., Adebowale, K.O., 2015b. Effects of time, soil organic matter, and iron oxides on the relative retention and redistribution of lead, cadmium, and copper on soils. Environ. Sci. Pollut. Res. 22 (13), 10331–10339.
Diagboya, P.N., Olu-Owolabi, B.I., Dikio, E.D., Adebowale, K.O., 2018. Concentration-dependent and simultaneous sorption and desorption of pyrene and fluorene on major soil minerals in sub-Saharan Africa. Appl. Clay Sci. 153, 257–264.
Freundlich, H.M.F., 1906. Über die adsorption in lösungen. Z. Phys. Chem. 57A, 385–470.
Hao, Y.M., Man, C., Hu, Z.B., 2010. Effective removal of Cu (II) ions from aqueous solution by amino-functionalized magnetic nanoparticles. J. Hazard Mater. 184 (1–3), 392–399.
Igberase, E., Osifo, P., Ofomaja, A., 2014. The adsorption of copper (II) ions by polyaniline graft chitosan beads from aqueous solution: equilibrium, kinetic and desorption studies. J. Environ. Chem. Eng. 2 (1), 362–369.
Kang, Y., Zhou, L., Li, X., Yuan, J., 2011. β-Cyclodextrin-modified hybrid magnetic nanoparticles for catalysis and adsorption. J. Mater. Chem. 21 (11), 3704.
Lagergren, S., 1898. Zur theorie der sogenannten adsorption gelöster stoffe. Kungliga Svenska Vetenskapsakademiens. Handlingar 24, 1–39.
Langmuir, I., 1916. The constitution and fundamental properties of solids and liquids. J. Am. Chem. Soc. 38, 2221–2295.
Li, T.T., Liu, Y.G., Peng, Q.Q., Hu, X.J., Liao, T., Wang, H., Lu, M., 2013. Removal of lead(II) from aqueous solution with ethylenediamine-modified yeast biomass coated with magnetic chitosan microparticles: kinetic and equilibrium modeling. Chem. Eng. J. 214, 189–197.
Lu, S.G., Xu, Q.F., 2008. Competitive adsorption of Cd, Cu, Pb and Zn by different soils of Eastern China. Environ. Geol. 57 (3), 685–693.
Nassar, N.N., 2010. Rapid removal and recovery of Pb(II) from wastewater by magnetic nanoadsorbents. J. Hazard Mater. 184 (1–3), 538–546.
Okoli, C.P., Diagboya, P.N., Anigbogu, I.O., Olu-Owolabi, B.I., Adebowale, K.O., 2017. Competitive biosorption of Pb(II) and Cd(II) ions from aqueous solutions using chemically modified moss biomass (Barbula lambarenensis). Environ. Earth Sci. 76 (1).
Olu-Owolabi, B.I., Alabi, A.H., Diagboya, P.N., Unuabonah, E.I., During, R.A., 2017. Adsorptive removal of 2,4,6-trichlorophenol in aqueous solution using calcined kaolinite-biomass composites. J. Environ. Manag. 192, 94–99.
Olu-Owolabi, B.I., Alabi, A.H., Unuabonah, E.I., Diagboya, P.N., Böhm, L., Düring, R.A., 2016a. Calcined biomass-modified bentonite clay for removal of aqueous metal ions. J. Environ. Chem. Eng. 4 (1), 1376–1382.
Olu-Owolabi, B.I., Diagboya, P.N., Okoli, C.P., Adebowale, K.O., 2016b. Sorption behaviour of pentachlorophenol in sub-Saharan tropical soils: soil types sorption dynamics. Environ. Earth Sci. 75 (24).
Olu-Owolabi, B.I., Diagboya, P.N., Unuabonah, E.I., Alabi, A.H., Düring, R.A., Adebowale, K.O., 2018. Fractal-like concepts for evaluation of toxic metals adsorption efficiency of feldspar-biomass composites. J. Clean. Prod. 171C, 884–891.
Russo, M.E., Di Natale, F., Prigione, V., Tigini, V., Marzocchella, A., Varese, G.C., 2010. Adsorption of acid dyes on fungal biomass: equilibrium and kinetics characterization. Chem. Eng. J. 162 (2), 537–545.

Şengil, İ.A., Özacar, M., 2009. Competitive biosorption of Pb^{2+}, Cu^{2+} and Zn^{2+} ions from aqueous solutions onto valonia tannin resin. J. Hazard Mater. 166 (2–3), 1488–1494.

Tian, H., Li, J., Shen, Q., Wang, H., Hao, Z., Zou, L., Hu, Q., 2009. Using shell-tunable mesoporous Fe3O4@HMS and magnetic separation to remove DDT from aqueous media. J. Hazard Mater. 171 (1–3), 459–464.

Wang, S., Wang, K., Dai, C., Shi, H., Li, J., 2015. Adsorption of Pb^{2+} on amino-functionalized core–shell magnetic mesoporous SBA-15 silica composite. Chem. Eng. J. 262, 897–903.

Weber, W.J., Morris, J.C., 1963. Kinetics of adsorption on carbon from solutions. J. Sanit. Eng. Division, Am. Soc. Civil Eng. 89, 31–60.

Zhang, M., Gao, B., Varnoosfaderani, S., Hebard, A., Yao, Y., Inyang, M., 2013. Preparation and characterization of a novel magnetic biochar for arsenic removal. Bioresour. Technol. 130, 457–462.

Zhu, Y., Hu, J., Wang, J., 2012. Competitive adsorption of Pb(II), Cu(II) and Zn(II) onto xanthate-modified magnetic chitosan. J. Hazard Mater. 221–222, 155–161.